World Scientific
www.worldscientific.com

Recent developments on the Casimir torque

Benjamin Spreng

Department of Electrical and Computer Engineering,
University of California, Davis, CA 95616, USA

Tao Gong

Department of Electrical and Computer Engineering,
Department of Materials Science and Engineering,
University of California, Davis, CA 95616, USA

Jeremy N. Munday*

Department of Electrical and Computer Engineering,
University of California, Davis, CA 95616, USA
jnmunday@ucdavis.edu

The Casimir force acts on nearby surfaces due to zero-point fluctuations of the quantum electromagnetic field. In the nonretarded limit, the interaction is also known as the van der Waals force. When the electromagnetic response of the surfaces is anisotropic, a torque may act on the surfaces. Here, we review the literature and recent developments on the Casimir torque. The theory of the Casimir torque is discussed in an explicit example for uniaxial birefringent plates. Recent theoretical predictions for the Casimir torque in various configurations are presented. A particular emphasis is made on experimental setups for measuring the Casimir torque.

Keywords: Casimir torque; van der Waals torque; anisotropic media.

PACS numbers: 03.70.+k, 42.50.Lc, 12.20.−m, 81.05.Xj

1. Introduction

The Casimir force exists between any pair of bodies separated by vacuum.[1] Generated by quantum fluctuations of the electromagnetic field, the force dominates at submicron separations, thus having practical implications for nano- and micro-electromechanical systems.[2,3] When retardation due to the finite speed of light can

---

*Corresponding author.

be neglected, the interaction is also known as the van der Waals force. While the Casimir force was originally predicted for ideal metal plates at zero-temperature,[4] the theory was soon extended to account for thermal fluctuations and boundary conditions imposed by real, homogeneous materials including an intervening medium between the two plates.[5, 6]

When the two plates are composed of anisotropic materials, the energy of the Casimir interaction depends on the mutual orientation of their optic axes. Consequently, besides the force appearing in isotropic systems, a torque causes a relative rotation of the two plates. While the Casimir force can be interpreted as a result of the radiation pressure of the vacuum modes, the Casimir torque can be given an interpretation of arising from angular momentum transfer from the vacuum modes to the plates.[7] The Casimir torque in the nonretarded limit was first predicted in Refs. 8 and 9. Retardation was fully taken into account for the first time in Ref. 10. Potential applications of the Casimir torque involve controlling rotation of small objects, for example in actuation of nano- and microelectromechanical systems.

Experimentally it has been difficult to measure the Casimir torque. The problem of parallelism can be avoided for measuring the Casimir force by replacing one of the plates by a sphere. However, for anisotropic materials the problem of parallelism cannot be avoided that simply, due to difficulties in achieving smooth spherical optically anisotropic materials. Recently, the Casimir torque was measured for the first time between a birefringent plate and a liquid crystal.[11]

In this paper, we review the recent developments on the Casimir torque (for earlier reviews see Refs. 12 and 13). In Sec. 2, we review the theoretical formalism of the Casimir interaction between two uniaxial anisotropic plates and discuss a few typical examples. Then, in Sec. 3, theoretical predictions on the Casimir torque in various systems are reviewed. We summarize the proposed experimental setups on measuring the Casimir torque in Sec. 4, while in Sec. 5, we review the experimental result, which verified the existence of the Casimir torque for the first time. Finally, we give concluding remarks in Sec. 6.

2. Casimir Interaction Between Anisotropic Plates

We review the theoretical formalism for the Casimir interaction between two uniaxial birefringent plates. Uniaxial birefringent plates are the simplest example for an optically anisotropic system as there is only one axis governing the anisotropy. All other directions are optically equivalent. As depicted in the inset of Fig. 1(a), we consider two semi-infinite plates separated by a distance d in an isotropic medium with dielectric function ε_3. The theory we present here can be straightforwardly extended to finite plate thickness or multilayered anisotropic plates using the transfer matrix method.[14–16] A flexible open-science software for calculating the Casimir interaction between anisotropic surfaces of various materials and shapes is also readily available.[17]
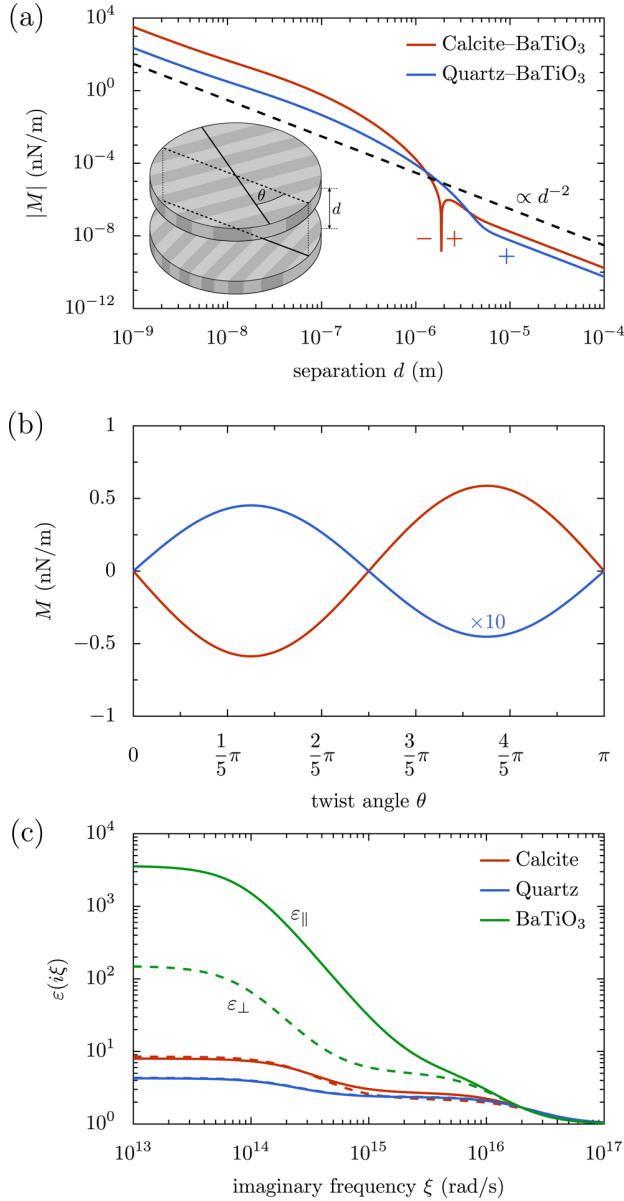
Fig. 1.   (Color online) Casimir torque between two birefringent plates at a separation d where the optic axes are at an angle θ. (a) Magnitude of the Casimir torque per area as a function of separation at $\theta = \pi/4$ for calcite (quartz) above a barium titanate plate in vacuum shown by the red (blue) line. The plus and minus indicate the sign of the torque, and the dashed line indicates a power law proportional to d^{-2}. (b) Casimir torque per area as a function of the angle between the optic axes at $d = 100$ nm for the same systems. The Casimir torque corresponding to the blue line is multiplied by a factor of 10 for visibility. (c) Dielectric functions of calcite, quartz and BaTiO$_3$ as a function of imaginary frequency ξ. For the birefringent dielectrics, the solid (dashed) lines correspond to $\varepsilon_{\parallel}$ ($\varepsilon_{\perp}$).

The z-axis of our reference system is chosen perpendicular to the plates, and the x-axis to be aligned with the optic axis of plate 1. The optic axis of plate 2 lies also in the x-y-plane but is twisted by an angle θ with respect to the optic axis of the other plate. The dielectric tensors of the two plates are then described by the matrices

$$
\boldsymbol{\varepsilon}_1 = \begin{pmatrix} \varepsilon_{1\|} & 0 & 0 \\ 0 & \varepsilon_{1\perp} & 0 \\ 0 & 0 & \varepsilon_{1\perp} \end{pmatrix},
$$

$$
\boldsymbol{\varepsilon}_2 = \begin{pmatrix} \varepsilon_{2\|}\cos^2\theta + \varepsilon_{2\perp}\sin^2\theta & (\varepsilon_{2\perp}-\varepsilon_{2\|})\sin\theta\cos\theta & 0 \\ (\varepsilon_{2\perp}-\varepsilon_{2\|})\sin\theta\cos\theta & \varepsilon_{2\|}\sin^2\theta + \varepsilon_{2\perp}\cos^2\theta & 0 \\ 0 & 0 & \varepsilon_{2\perp} \end{pmatrix},
$$
(1)

where the subscripts $\|$ and $\perp$ denote the components of the dielectric tensor parallel and perpendicular to the optic axes. Note that the components of the dielectric tensor are in general dispersive and depend on the angular frequencies of the electromagnetic waves.

Within the scattering formalism,[18,19] the Casimir free energy of the system at temperature T is then given by[20,21]

$$
\mathcal{F}(d,\theta) = \frac{k_{\mathrm{B}}T}{4\pi^2} \sum_{n=0}^{\infty}{}' \int_0^{2\pi} d\varphi \int_0^{\infty} dk\, k \log\det(\mathbf{1} - \mathbf{r}_1\mathbf{r}_2 e^{-2\rho_3 d}),
$$
(2)

where the summand is evaluated at imaginary frequencies $\xi_n = 2\pi n k_{\mathrm{B}}T/\hbar$ and the prime indicates that the $n=0$ term is weighted by a factor of $1/2$. The integration variables k and φ are the radial and angular wave-vector components within x-y-plane of the plane-waves reverberating between the two surfaces. The imaginary part of the z-component of the wave vectors in the medium is given by

$$
\rho_3 = \sqrt{\varepsilon_3 K_n^2 + k^2}
$$
(3)

with the imaginary vacuum wave number $K_n = \xi_n/c$.

For each plate $i = 1, 2$, $\mathbf{r}_i$ represents the reflection matrix on its surface, and it can be written as[22,23]

$$
\mathbf{r}_i = \frac{1}{r_{\mathrm{D}}} \begin{pmatrix} r_{ss,\mathrm{N}} & r_{sp,\mathrm{N}} \\ r_{ps,\mathrm{N}} & r_{pp,\mathrm{N}} \end{pmatrix}
$$
(4)

with

$$
\begin{aligned}
r_{sp,\mathrm{N}} &= r_{ps,\mathrm{N}} = K_n\sqrt{\varepsilon_3}\varepsilon_{i\perp}\rho_i\rho_3(\rho_i - \tilde{\rho}_i)\sin(2\theta_i), \\
r_{ss,\mathrm{N}} &= \sin^2(\theta_i)\tilde{\alpha}_-\gamma_+ + \cos^2(\theta_i)\alpha_-\nu_+, \\
r_{pp,\mathrm{N}} &= -\sin^2(\theta_i)\tilde{\alpha}_+\gamma_- + \cos^2(\theta_i)\alpha_+\nu_-, \\
r_{\mathrm{D}} &= \sin^2(\theta_i)\tilde{\alpha}_+\gamma_+ + \cos^2(\theta_i)\alpha_+\nu_+,
\end{aligned}
$$
(5)

where

$$\alpha_\pm = \rho_3 \pm \rho_i,$$

$$\tilde{\alpha}_\pm = \rho_3 \pm \tilde{\rho}_i,$$

$$\nu_\pm = \varepsilon_3 \rho_i^3 \pm \varepsilon_{i\perp} \rho_i \tilde{\rho}_i \rho_3,$$

$$\gamma_\pm = \varepsilon_{i\perp} K_n^2 (\varepsilon_{i\perp} \rho_3 \pm \varepsilon_3 \rho_i).$$

$$(6)$$

and

$$\rho_i = \sqrt{\varepsilon_{i\perp} K_n^2 + k^2},$$

$$\tilde{\rho}_i = \sqrt{\varepsilon_{i\parallel} K_n^2 + k^2 + (\varepsilon_{i\parallel}/\varepsilon_{i\perp} - 1)k^2 \cos^2 \theta_i}.$$

$$(7)$$

Due to the anisotropy of the plates, the reflection matrices (4) are nondiagonal with respect to s and p polarization. Because we chose the extraordinary axis of the first birefringent plate along the x-axis, we have $\theta_1 = \varphi$ and $\theta_2 = \varphi + \theta$ when using the reflection matrices (4) in the formula for the Casimir free energy (2).

Note that formula (2) gives more physical insights compared to Barash' original result[10, 24, 25] which is somewhat cumbersome. It has been shown that both formulas are equivalent.[21] An alternative derivation can be found in Ref. 26, which pointed out a misprint in Refs. 10 and 24. Furthermore, the formula for the Casimir free energy (2) can be straightforwardly extended for multi-layered systems or plates of finite thickness by using the corresponding reflection matrix for those interfaces.

The Casimir pressure $P(d, \theta)$ between the two plates is given by the negative derivative of the free energy with respect to separation

$$P(d, \theta) = -\frac{\partial \mathcal{F}(d, \theta)}{\partial d}.$$

$$(8)$$

Using Jacobi's formula from matrix calculus, we can derive an explicit formula for the Casimir pressure and find

$$P(d, \theta) = \frac{k_\mathrm{B} T}{2\pi^2} \sum_{n=0}^{\infty}{}' \int_0^{2\pi} d\varphi \int_0^\infty dk\, k\rho_3 \operatorname{tr}[(\mathbf{1} - \mathbf{r}_1 \mathbf{r}_2 e^{-2\rho_3 d})^{-1} \mathbf{r}_1 \mathbf{r}_2 e^{-2\rho_3 d}].$$

$$(9)$$

Likewise, a formula for the Casimir torque per unit area

$$M(d, \theta) = -\frac{\partial \mathcal{F}(d, \theta)}{\partial \theta},$$

$$(10)$$

can be derived. The formula then reads

$$M(d, \theta) = \frac{k_\mathrm{B} T}{4\pi^2} \sum_{n=0}^{\infty}{}' \int_0^{2\pi} d\varphi \int_0^\infty dk\, k \operatorname{tr}[(\mathbf{1} - \mathbf{r}_1 \mathbf{r}_2 e^{-2\rho_3 d})^{-1} \mathbf{r}_1 \partial_\theta \mathbf{r}_2 e^{-2\rho_3 d}]$$

$$(11)$$

for which the derivative of the reflection matrix on plate 2 with respect to the twist angle θ is required. From Eq. (4) and using that $\theta_2 = \varphi + \theta$, an expression for $\partial_\theta \mathbf{r}_2$ can be straightforwardly derived.

In general, the integrals in Eq. (11) have to be evaluated numerically. Under certain conditions, the formula for the Casimir torque can, however, be simplified

considerably. For instance, when the retardation of the Casimir interaction can be neglected and the birefringendhe torque becomes[10, 24]

$$M(d, \theta) \approx -\frac{\alpha}{64\pi^2 d^2} \sin(2\theta) \tag{12}$$

with

$$\alpha = -2\pi k_{\mathrm{B}} T \sum_{n=0}^{\infty} {}' \frac{(\varepsilon_{2\parallel} - \varepsilon_{2\perp})(\varepsilon_{1\parallel} - \varepsilon_{1\perp})\varepsilon_3^2}{(\varepsilon_{1\perp}^2 - \varepsilon_3^2)(\varepsilon_{2\perp}^2 - \varepsilon_3^2)}$$
$$\times \log\left(1 - \frac{(\varepsilon_{1\perp} - \varepsilon_3)(\varepsilon_{2\perp} - \varepsilon_3)}{(\varepsilon_{1\perp} + \varepsilon_3)(\varepsilon_{2\perp} + \varepsilon_3)}\right), \tag{13}$$

where the dielectric functions are evaluated at the imaginary Matsubara frequencies $i\xi_n$. In the above limits, the Casimir torque is thus inversely proportional to the second power of the separation d and proportional to $\sin(2\theta)$. As we will see in the examples below, this behavior is typical even if the limiting criteria are not met (see results for the Casimir torque in Figs. 1(a) and 1(b)).

To illustrate the Casimir interaction between two anisotropic plates, we consider a calcite (quartz) plate and a barium titanate plate in vacuum at room temperature $T = 300$ K. The dielectric functions of the plates are modeled according to Ref. 24. The results for the magnitude of the Casimir torque per area as a function of separation for a fixed twist angle $\theta = \pi/4$ are depicted as the solid red (blue) lines in Fig. 1(a). For both configurations, the Casimir torque is asymptotic to the power law d^{-2} (dashed line) for short and large separations. For short separations, retardation can be neglected and the power law is explained by formula (12). When the separation is large compared to the thermal wavelength $\lambda_T = \hbar c/k_{\mathrm{B}} T$, the zero-frequency Matsubara contribution for the Casimir torque dominates. Because for dimensional reasons the in-plane wave vector component k appearing as the integration variable in Eq. (11) scales inversely proportional to the separation d, we expect that for separations larger than $\lambda_T = 7.6\ \mu$m at room temperature the Casimir torque behaves like d^{-2} in agreement with our observations. It is interesting to note that the Casimir torque is thus of larger range than the Casimir pressure which scales as d^{-3} for large separations.[1]

While the Casimir torque is always positive for the configuration with quartz, the torque for the calcite configuration undergoes a sign change from negative to positive at a separation of about 1.87 μm. A positive torque at the twist angle $\theta = \pi/4$ means that it tends to align the optic axes of the two plates, while a negative torque at the same twist angle rotates the plates such that the optic axes become perpendicular. The sign of the Casimir torque can be understood by comparing the components of the dielectric tensors of the two plates. For the two configurations considered here, Fig. 1(c) shows those components as a function of imaginary frequency. The solid lines (dashed) lines correspond to $\varepsilon_\parallel$ ($\varepsilon_\perp$). From Eq. (12), we see that the sign of each imaginary frequency contribution is proportional to the product $(\varepsilon_{2\parallel} - \varepsilon_{2\perp})(\varepsilon_{1\parallel} - \varepsilon_{1\perp})$ which is proportional to the product of birefringence of

the two plates. When the medium is vacuum, i.e. $\varepsilon_3 = 1$, the logarithm in Eq. (13) yields a negative number. Thus, in the examples considered here, the sign of the Casimir torque is opposite to the sign of the product of birefringence.

At large separations the zero-frequency Matsubara term dominates. Because at low frequencies the product of the birefringence is negative for both configurations, the Casimir torque is then positive in both cases. As the separation between the two plates decreases, higher frequencies contribute to the Casimir interaction. The sign of the Casimir torque for the configuration with quartz has the same sign over all separations because the sign of the birefringence of quartz and BaTiO$_3$ is the same over all frequencies. In contrast, the birefringence of calcite undergoes a sign change at about 2.7×10^{14} rad/s, which explains the change of sign towards shorter separations for the Casimir torque in the corresponding configuration.

3. Theoretical Predictions

In this section, we review the theoretical predictions made for the Casimir torque in various proposed systems. Effects of anisotropy of the Casimir interaction between two surfaces are in general a consequence of either the electromagnetic response of the material they are composed of or their morphology (see Fig. 2) or possibly a combination of both. The contributions to the Casimir interaction due to shape and material anisotropy have been extensively studied in Ref. 27. We split our review of the theoretical predictions into those two categories in the following.

3.1. *Material response anisotropy*

While it is generally known that retardation and intervening dielectric media decrease the Casimir interaction between isotropic surfaces, it has been found in Ref. 20 that the opposite is true for anisotropic surfaces. As can be seen in Fig. 3(a),
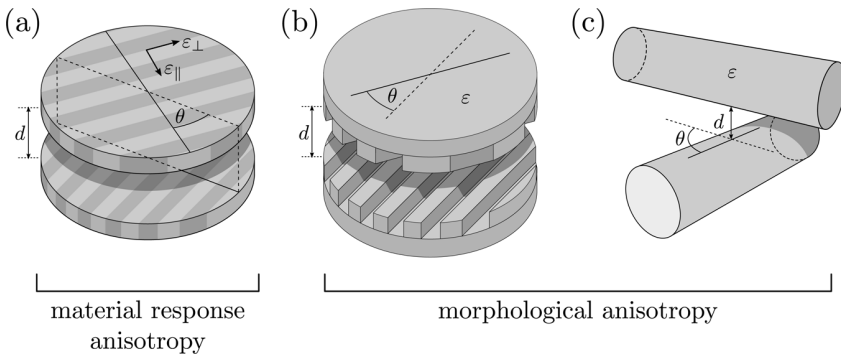

Fig. 2. Optical anisotropy due to the material response or the morphology of the interacting surfaces. (a) Plates with an anisotropic crystalline structure yield an anisotropic electromagnetic response. Examples with morphological anisotropy are (b) nanostructured surfaces like lamellar gratings and (c) cylindrical surfaces. In all examples, a Casimir torque as a function of the separation d exists when the objects are misaligned by a relative twist angle θ.

the Casimir torque between two TiO_2 plates is enhanced when retardation is included in the calculation. Moreover, when water is considered as an intervening dielectric medium, the Casimir torque can be surprisingly increased by a factor of two.

The Casimir torque can be also enhanced by more than an order of magnitude when coating the interacting surfaces with a graphene layer.[31] Tunability of the torque using multilayer stacks of anisotropic media with respect to the relative optic axes and layer thicknesses has been investigated in Ref. 14.

In Ref. 29, the Casimir torque between two biaxially anisotropically polarizable slabs of finite thickness is studied. Both optic axes are considered to be within the planes of the interacting slabs. It is found that, when the polarizabilities along the two optic axes are equal at a given frequency ω_c, the Casimir torque changes sign at a separation $d_c \sim c/2\omega_c$ (see Fig. 3(b)). This effect is illustrated for black phosphorus and phosphorene, where the sign reversal occurs at separations of tens of nanometers. A further study showed that the presence of extra charge carriers in black phosphorus and the presence of an intervening fluid between the plates, can both enhance the magnitude of the Casimir torque.[32]

The Casimir torque between two Weyl semimetals has been studied in Ref. 30. In this system, the Casimir torque is generated by a chiral anomaly in the topological Weyl semimetals, which is a completely different mechanism compared to birefringent plates. As one can see from the results depicted on the left of Fig. 3(c), the chiral anomaly is manifested by showing a $\sin(\theta)$-dependence for the torque at short separations (upper curves), while the typical $\sin(2\theta)$-dependence appears for large separations (lower curves). On the right side of Fig. 3(c), the resulting maximum value of the Casimir torque is compared to ordinary birefringent plates. It is found that the magnitudes of the torque are similar, but the large-distance behavior for Weyl semimetals is at least an order of magnitude larger at a separation of one micron and higher.

In Ref. 33, the Casimir torque and force between uniaxial anisotropic topological insulator slabs have been investigated in the nonretarded limit. Interestingly, it has been found that the Casimir force can be tuned from attractive to repulsive depending on the angle between the optic axes of the two slabs. The Casimir torque in this system is, however, rather small compared to dielectric anisotropic slabs and thus topological insulator slabs are not suited for measuring the Casimir torque at this time.

Another interesting set of anisotropic materials that have been studied in the context of the Casimir torque are photonic topological insulators.[34] Not only do photonic topological insulators have a distinguished optic axis like birefringent crystals, but the axis also possesses a preferred direction. As a consequence the Casimir torque between photonic topological insulator plates is thus not π-periodic, but rather 2π-periodic instead. By applying an external magnetic field, the direction and strength of the torque can be driven allowing control of the relative rotation of the two plates.
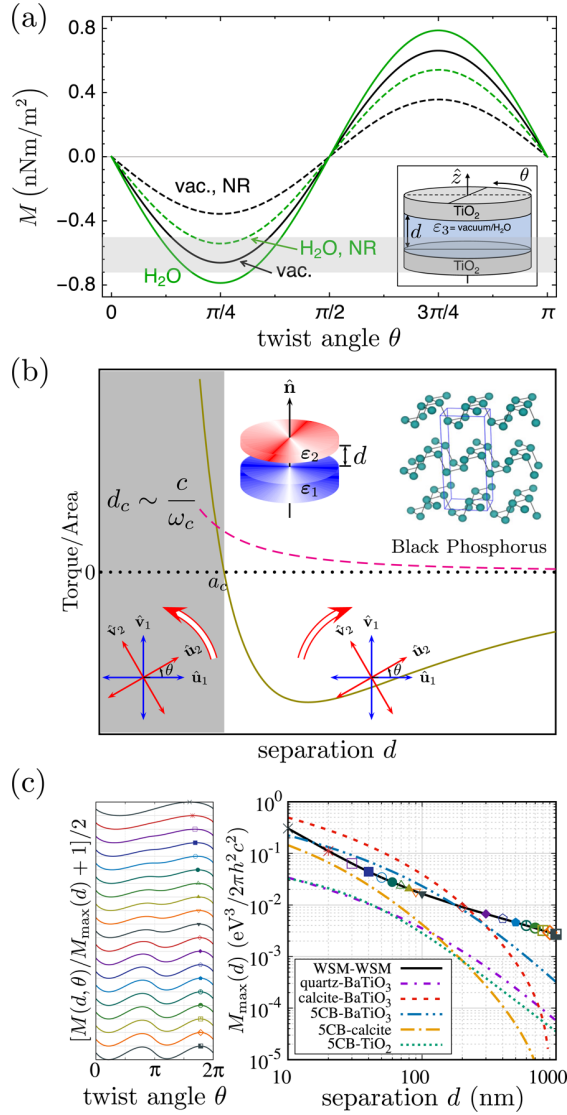
Fig. 3. (Color online) Predictions for the Casimir torque. (a) Casimir torque between TiO_2 plates with water or vacuum as the intervening dielectric medium at a separation of 30 nm (taken from Ref. 28). The green (black) lines correspond to the results for water (vacuum). The dashed lines are results in the nonretarded limit (NR) and the solid lines take retardation into account. (b) Distance-dependent sign reversal of the Casimir torque (taken from Ref. 29). The solid line shows the Casimir torque between two black phosphorus surfaces (see inset) at the relative angle $\theta = \pi/4$. The dashed curve corresponds to the result in the nonretarded limit. (c) Chiral-anomaly-driven Casimir torque between Weyl semimetals (taken from Ref. 30). Left: Normalized Casimir torque as a function of twist angle θ for various separations. The labels mark the maximum value of the torque, which is used on the figure on the right. Right: Maximal Casimir torque as a function of separation. The result between two Weyl semimetals is depicted as the black line. The dashed lines correspond to the Casimir torque between various birefringent materials. All results are calculated at zero temperature.

When an external magnetic field is applied to a III–IV semiconductor such as InSb, an optical anisotropy can be induced for the dielectric tensor. Magnetic fields of 1 T can then lead to Casimir torques between plates of such materials, which become comparable to that of permanent anisotropic materials.[35]

Magnetic materials have also been studied in the context of the Casimir torque. If an isotropic permeability is added to the anisotropic permittivity, the Casimir torque becomes larger at smaller separations and smaller at larger separations compared to nonmagnetic anisotropic plates.[36] The Casimir interaction between plates where also the permeability is anisotropic has been studied in Ref. 37. A three-layer structure composed of anisotropic saturated ferrite slabs with such properties has been studied in Ref. 15. The nontrivial magnetic permeability of the magnetodielectric slabs can be tuned by an externally applied magnetic field. It is shown that this setup can be used to design a switch for the Casimir torque for an anisotropic plate placed between two other anisotropic plates. When the optic axes of the outer two plates are perpendicular to each other, the torque acting on the middle plate from the two outer plates is opposite in sign thus effectively canceling out. On the other hand, when the optic axes of the outer plates are aligned, the torque on the intermediate layer is turned on.

It has been further found that the Casimir torque plays a major role in the formation of $BaTiO_3$ mesocrystals in an aqueous solution. Mesocrystals are an aggregate of nanocrystals where crystal axes are aligned. For cubic or spherical $BaTiO_3$ nanocrystals, it has been shown that the attachment of particles with alignment of their crystal axes is caused by the Casimir torque as the main mechanism when their size is smaller than 5 nm.[38] For larger crystals, the electric dipole–dipole interaction dominates.

The application of the theory of Casimir torques to liquid crystals is a further point of interest. Because of the small elastic constant of nematic liquid crystals, the Casimir interaction between a birefringent plate causes a distortion of the ordered structure of the liquid crystal. This effect has been first studied in Ref. 39 in the nonretarded limit and an experimental proposal was made. More recently, another experimental proposal for measuring the Casimir torque on liquid crystals was made including predictions on the torque where retardation was taken into account[40] which ultimately lead to the first experimental measurement of the Casimir torque[11] (see Sec. 5). In comparison to nematic liquid crystals, the Casimir torque between a cholesteric liquid crystal and a birefringent plate deviates significantly from the usual sinusoidal form as a function of the twist angle and decreases more slowly as a function of separation, potentially allowing for a measurement of the torque at larger separations.[16]

3.2. *Morphological anisotropy*

In the previous section, we have discussed the Casimir torque in a system where the two interacting surfaces are planar and composed of an anisotropic medium.

When the interacting surfaces are made of isotropic media, their geometric shapes can still induce an effective anisotropic electromagnetic response.

For instance, two periodically structured surfaces exhibit a Casimir torque when the direction of the periods is twisted by an angle θ. In Refs. 43 and 44, the Casimir torque between two periodically corrugated plates has been studied. It was found that for corrugation periods and amplitudes typical for Casimir experiments, the torque is much larger than the one found between planar anisotropic surfaces. For example, the torque per area at a separation of $d = 100$ nm is found to be 5.2×10^{-7} N m^{-1}, which is three orders of magnitude larger than the corresponding torque between calcite and BaTiO$_3$ as shown in Fig. 1(a). Moreover, the Casimir torque does not follow the usual sinusoidal behavior as a function of the twist angle in such systems.

A much larger torque compared to anisotropic planar surfaces has also been found between two lamellar gratings as depicted in Fig. 2(b). In Ref. 45, such system of two infinite lamellar gratings was studied for which the Casimir torque is obtained per unit area. As a result, the torque between two finite gratings can be approximated by multiplying the so-obtained result by the area of the interacting surfaces. This approximation will become valid when the lateral size of the plates is large enough compared to their separation and the gratings' characteristic length scales. Alongside their theoretical predictions, the authors of Ref. 45 proposed an experimental setup for measuring the Casimir torque between the two nanostructured plates, which will be discussed in Subsec. 4.3.

Interestingly, it has been found that for finite-sized gratings, the Casimir torque can be much larger than intuitively expected. In Ref. 41, the Casimir torque between such finite-sized gratings of circular and square shapes has been studied. The result for the Casimir torque per area at a fixed separation of $d = 100$ nm as a function of the twist angle θ is depicted in Fig. 4(a). While the torque for the infinite system is always negative in the figure, it undergoes several sign changes for the finite gratings. At smaller twist angles, the two finite gratings show qualitatively similar behavior when the number of repetitions n of the period length is equal. It is remarkable that the maximal torque per area for finite gratings is more than an order of magnitude larger than for the corresponding infinite system. For instance, the ratio between the maximal torque per area between the circular (square) grating and the infinite grating is 60 (50) for $n = 10$.

The appearance of this giant torque for finite gratings can be understood as follows. While the grating lines of the interacting surfaces cross each other infinitely times for infinite gratings at any nonzero twist angle $\theta \neq 0$, the number of crossings for finite gratings depends on the twist angle. Most crossings occur at a relatively small angle for which then the torque is maximal. In agreement with the numerical results shown in Fig. 4(a), the maximal torque should then increase with the number of repetitions n of the period length as long as the gratings are small enough. The authors of Ref. 41 argue that the giant torque for finite gratings is reminiscent of the fact that the Casimir interaction between infinite gratings undergoes
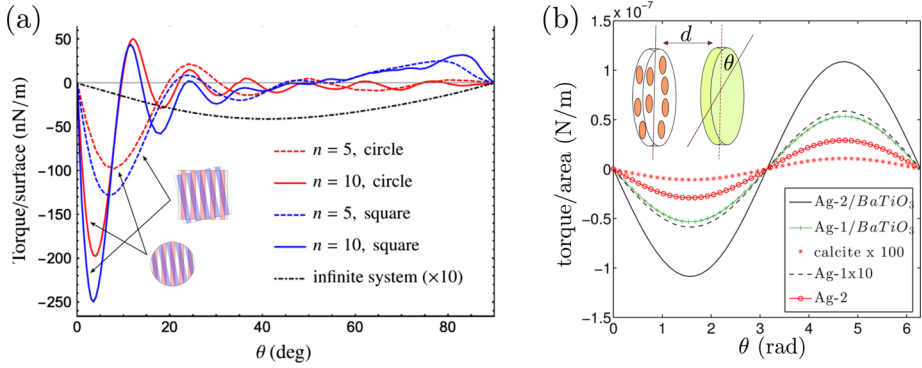
Fig. 4. (Color online) Predictions for the Casimir torque between surfaces with morphological anisotropy. (a) Casimir torque per unit area between rotated gratings as a function of twist angle θ (taken from Ref. 41). The colored lines correspond to finite gratings while the black dashed lines correspond to an infinite grating for which the result is multiplied by a factor of 10 for visibility. The finite systems' results are shown for $n = 5$ and $n = 10$ repetitions of the grating periods. See text for the dimensions of the gratings. (b) The nonretarded Casimir torque per area between slabs composed of planar arrays of nanoparticles (see inset) as a function of the twist angle θ at a separation $d = 20$ nm (adapted from Ref. 42). The black solid and green curves are the result of an aligned array of Ag nanospheres (Ag-1) and nanorods (Ag-2) interacting with a $BaTiO_3$ surface, respectively. The black dashed line is the result for two Ag-1 surfaces (multiplied by a factor of 10) and the red curves with circles represent the results for two Ag-2 surfaces. For a comparison, the torque between two calcite surfaces is depicted as the star symbols (multiplied by a factor of 100 for visibility). The medium in all scenarios is water.

a critical zero-order transition between a 2D-periodic system at $\theta \neq 0$ and a 1D-periodic system at $\theta = 0$. This critical zero-order transition between the infinite gratings exemplifies in the Casimir free energy having a discontinuous jump at $\theta = 0$ which the authors call the $\theta = 0$ anomaly. The Casimir torque associated with this discontinuous jump in the free energy is then technically infinite, which is coherent with the observation that the maximal torque increases with the grating size.

A Casimir torque can also appear between cylindrical objects like wires and rods as depicted in Fig. 2. The Casimir torque between anisotropic cylindrical thin rods in the nonretarded limit was first studied in Ref. 46. The results are derived from the interaction between two composite media in which the rods are embedded. When the composite media are sufficiently dilute, the torque between two individual rods can be determined by assuming pairwise additivity of the interaction. In a similar way, the Casimir torque between cylinders and a cylinder and an anisotropic planar wall were studied in Ref. 47, whereas retardation effects in the theory were included in Ref. 48. The exact Casimir interaction between two crossed perfectly reflecting cylinders has been studied in Ref. 49.

Because the torque between semiconducting rods is of longer range than for metals, carbon nanotubes may be a good candidate for measuring the Casimir torque between cylindrical objects.[50] Composite media with embedded nanorods may, however, be better suited for an experimental measurement as the torque is

generally much larger and in particular orders of magnitude larger than for ordinary anisotropic plates.[27,51] As shown in Fig. 4(b), the interaction between a surface composed of embedded nanoparticles and a birefringent plane also exhibits a strong Casimir torque.[42]

Another application of the Casimir torque is that it can mediate an efficient noncontact transfer of angular momentum between spherical nanoparticles bringing new opportunities for the control of nanomechanical devices. In Ref. 53, the dynamics of chains of rotating nanoparticles with an arbitrary number of elements has been studied. It has been shown that synchronization of the nanoparticles' angular velocities occurs within seconds for structures with realistic dimensions. Moreover, exotic behaviors of the chain have been predicted, such as "rattleback"-like dynamics, for which the sense of rotation of a particle changes several times before synchronization, and configurations in which angular momentum is not transferred to a selected particle. For an externally driven nanoparticle chain, the authors of the aforementioned article have established a condition for which an efficient transfer of angular momentum can be achieved.

Plates of isotropic materials can also exhibit a Casimir torque when they are finite in lateral size and their surfaces are titled with respect to each other. In this case, the torque on the plates is not a result of the transfer of angular momentum of the vacuum modes on the plate as in the examples discussed above. The torque is rather a result of an imbalance of the Casimir force acting on different parts of the plate. The direction of the torque is in the plane of the tilted plate and the torque acts in such a way that it increases the tilt. The nontrivial interplay of geometry and temperature for inclined plates has been studied in Ref. 54. The Casimir torques between titled plates play an important role for electrostatic torsional actuators, which find application in nano- and microelectromechanical systems.[55] As illustrated in Fig. 5(a) the total torque acting on such electrostatic torsional actuators is the sum of torques due to the Casimir force, the electrostatic force, and the restoring torque M_{res} of the torsional beam. While the electrostatic force can be switched off by setting the applied potential to zero, the Casimir force will always
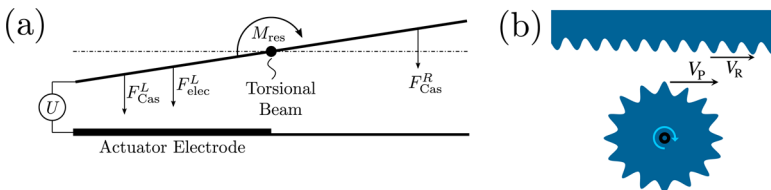

Fig. 5. (a) Schematic setup of an electrostatic torsional actuator. The Casimir force F_{Cas} and electrostatic force F_{elec} act on a plate fixed on a torsional beam. Both forces together with the restoring torque M_{res} give rise to the total torque acting on the plate which determines the dynamics of the actuation. The electrostatic force can be controlled by an applied potential U. (b) Noncontact gear mediated by the Casimir interaction. The moving rack with velocity v_{R} induces a velocity v_{P} on the pinion mediated by the Casimir interaction (taken from Ref. 52).

be present and influence the dynamics of the actuator. A detailed study on the sensitivity of the materials' optical properties of single-beam and double-beam torsional Casimir actuators can be found in Refs. 56–58.

Moreover, the idea of using the Casimir interaction for noncontact gears has been put forward as a periodically corrugated surface induces a torque on a corrugated cylinder in front of it[52] (see Fig. 5(b)). The torque acting on the pinion in this case is a result of the lateral Casimir force. This concept of noncontact gears has been further studied for two concentric cylindrical gears.[59–62] Such noncontact gears are by design virtually wear-proof and could help towards making more durable machine parts in nano- and micromechanical systems.

Furthermore, the Casimir torque can be exploited to induce alignment of ellipsoidal particles inside spheroids[63] or CO_2 molecules in front of a graphene plane.[64] Such a vertical alignment of CO_2 molecules may allow them to pass through a graphene membrane. This mechanism may be exploited to improve the performance of CO_2 separation membranes useful for an efficient atmospheric CO_2 reduction.

4. Proposed Experiments

In the past, several experimental setups to measure the Casimir torque have been proposed. In this section, we review those proposed experiments. In the following section, the setup which allowed for a measurement of the Casimir torque for the first time will be discussed.

4.1. *Floating birefringent plate over a barium titanate crystal*

In Ref. 24, a system composed of a quartz or calcite disk above a $BaTiO_3$ plate immersed in ethanol was proposed to measure the Casimir torque. The experimental setup is depicted in Fig. 6(a). With the intervening liquid, the Casimir interaction is attractive for separations shorter than a few nanometers, but it is repulsive for larger separations. This repulsive Casimir force is counterbalanced by the net weight of the disk leading to a stable equilibrium point at a certain separation. For a disk with 40 μm diameter and 20 μm thickness, the equilibrium separation was found to be at about 100 nm for both configurations. This equilibrium separation can be tailored to experimental needs by changing, for instance, the disk thickness.

Placing the birefringent disk at the equilibrium separation, it can rotate freely in a sort of frictionless bearing. With a 100 mW laser, the rotation of the disk can be controlled by transferring the angular momentum of the light to the disk. The light-induced rotation can be stopped using a shutter and the position of the disk can be monitored by means of a microscope objective coupled to a CCD camera for imaging.

Using the laser light, the twist angle between the optic axes of the birefringent crystals can be rotated until $\theta = \pi/4$. Once the laser beam is shuttered, the disk then rotates towards the configuration of minimum energy. The rotational motion
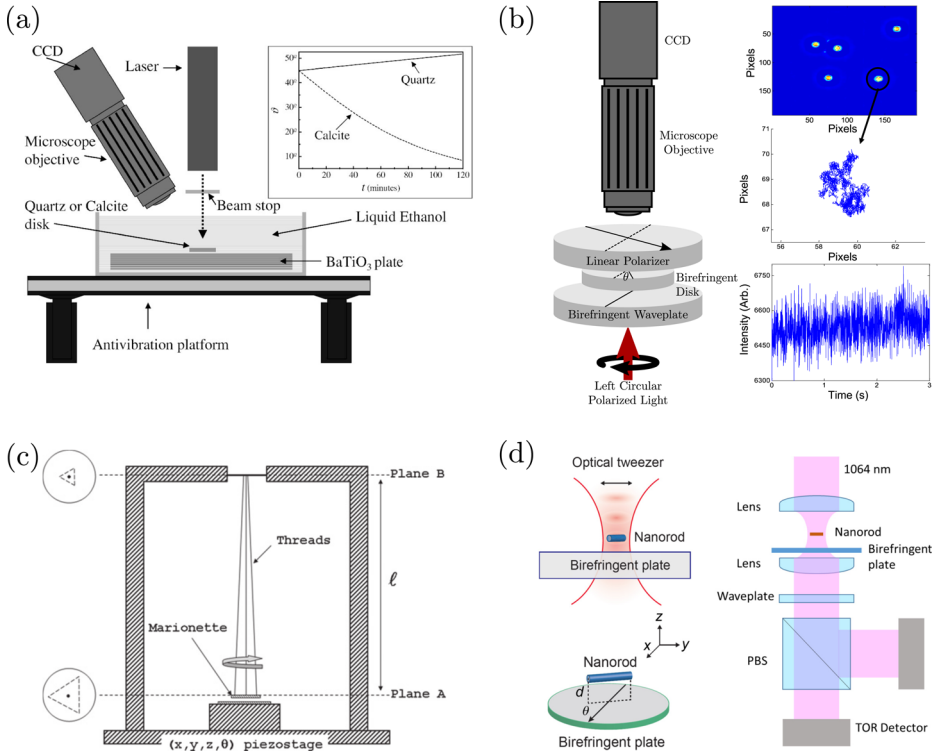
Fig. 6. Proposed experiments for measuring the Casimir torque. (a) Experimental setup of a floating quartz or calcite disk in ethanol above a BaTiO$_3$ plate (taken from Ref. 24). Inset: Time evolution for a starting angle of $\theta = \pi/4$. (b) Influence of Brownian motion on the Casimir torque of a floating plate (taken from Ref. 65). Left: experimental setup. Right: computerized tracking and intensity fluctuations for 10 μm polystyrene sphere from early calibration procedures. From top to bottom: CCD image and determination of particle centers, tracking of one sphere over 5 s and intensity fluctuations of scattered light. (c) Three-threaded torsion pendulum for measuring the Casimir torque. One plate is suspended by the pendulum, while the other is attached to a piezo-stage (taken from Ref. 45). (d) Top left: Nanorod trapped using an optical tweezer above a birefringent plate (taken from Ref. 66). Bottom left: relative orientation of the nanorod and the optic axis of the birefringent plate. Right: Schematic experimental setup for detecting the torsional (TOR) vibration of the levitated nanorod.

of the disk is then governed by the equation of motion for the twist angle

$$I\ddot{\theta} + \frac{\pi}{2}\frac{R^4}{d}\eta\dot{\theta} = a\sin(2\theta) \tag{14}$$

with radius of the disk R, its momentum of inertia I, the viscosity of ethanol $\eta = 1.2 \times 10^{-3}$ Ns/m^2, the separation between plate and disk d and the Casimir torque $a\sin(2\theta)$.

The time evolution can then be estimated by determining a from a fit to the Casimir torque calculated using formula (11) and solving (14) for $\theta(t = 0) = \pi/4$ and $\dot{\theta}(t = 0) = 0$. The results for the proposed experimental configuration are

depicted in the inset of Fig. 6(a). As the motion is overdamped, the disk rotates slowly towards the angle of minimal energy. After a few minutes, the rotation due to the Casimir torque can be observed. Because the calcite configuration rotates quicker, it is more likely to show a noticeable effect in the experiment.

The experiment may be further optimized using other dimensions of the disk or making the disk heavier to bring the equilibrium separation closer to the plate and thus increasing the Casimir torque. Another possibility is to use a different liquid with a smaller viscosity to significantly increase the angular velocity of the disk.

Due to the presence of the intervening liquid, Brownian motion needs to be taken into account when describing the experimental configuration. The authors of Ref. 24 argue that for the vertical direction Brownian motion can be neglected as a displacement of a few nanometers from the equilibrium separation would require a force of the order of 0.1 nN corresponding to an energy equal to 600 meV, which is more than one magnitude larger than the thermal energy $k_{\mathrm{B}}T$ (about 25 meV at room temperature). For the rotational motion, the effect of Brownian motion is more noticeable. While the driving torque for the calcite plate is estimated to be about 5 times larger than the one associated with thermal fluctuations, Brownian and quantum electrodynamical torques are of the same order of magnitude for the quartz plate. An accurate statistical analysis of a large number of experiments should nevertheless allow an observation of the Casimir torque even in the system with the quartz disk.

Experimentally, this scheme has proven somewhat difficult as has been pointed out in Ref. 65. One problem is that within the rather long time scales of tens of minutes, the disks can easily encounter contaminants causing them to stop floating. Another complication is the alignment of laser optics in real time as the disk moves.

4.2. *Casimir torque in the presence of Brownian motion*

The slow rotational speeds due to the damping of the viscous fluid in the proposed experiment of the previous section make it rather difficult to observe the Casimir torque. As the second term on the left-hand side of Eq. (14) shows, the damping term is proportional to the fourth power in the radius of the disk, $\propto R^4$. The authors of Ref. 65, thus propose to reduce the surface area of the disks to increase the rotational speeds. The energy scale of the Casimir torque will then, however, become comparable to thermal energy $k_{\mathrm{B}}T$. Brownian motion will therefore become more important as the disk radius decreases. The rotational diffusion coefficient D_r sets the timescale of the Brownian rotation. For a disk with radius $R = 1~\mu$m, it is given by $D_r \simeq 3k_{\mathrm{B}}T/32\eta R^3 \approx 0.39$ rad s^{-1} for $\eta = 1.0 \times 10^{-3}$ N s m^{-2}. A wall in close proximity of the disk will further reduce the value of the rotational diffusion coefficient.

In the regime where the torque due to thermal fluctuations becomes comparable to the one due to quantum fluctuations, the disk will no longer rotate smoothly

back to the configuration of minimal energy. The twist angle between optic axes will instead fluctuate and sample all angles. The probability distribution $p(\theta)$ for the observation of the twist angle θ is then given by the Boltzmann distribution

$$p(\theta) = \alpha \exp(-\mathcal{F}(d,\theta)/k_{\mathrm{B}}T), \tag{15}$$

where $\mathcal{F}(d,\theta)$ is the Casimir free energy (2) and α is a normalization constant such that $\int p(\theta)\mathrm{d}\theta = 1$. An observation of the angle between the optic axes as a function of time, allows one to then deduce the probability distribution and from that the Casimir free energy associated to the torque.

The experimental apparatus proposed to conduct this experiment is depicted in Fig. 6(b). While in the previous section a repulsive Casimir force was used to levitate the disk from the birefringent plate, another levitation scheme is suggested in Ref. 65. The main reason for not using the Casimir repulsion is that its existence had not been experimentally verified at that time, but only 3 years later.[67] Instead double-layer repulsion was proposed as an adjustable levitation scheme, which is commonly used in colloidal suspensions. A strong double-layer between the plate and disk can be induced by adding a surfactant (e.g. sodium dodecyl sulfate (SDS)) to an aqueous solution. The surfactant molecules attach to the interacting surfaces causing a charge buildup of the same sign on the plate and disk. This results in a repulsive electrostatic force for which the Debye screening length can then be adjusted by adding an electrolyte (e.g. NaCl) to the solution. In the aqueous system, the disk will then reside at an equilibrium separation determined by the balance between the Casimir force, the double-layer force, and the disk's weight. While the Casimir force and the weight of the disk are set by the geometry of the disk, the double-layer force can be adjusted by changing the electrolyte strength and concentration. For a circular $LiNbO_3$ disk with radius $R = 1$ μm and height $h = 0.5$ μm above a calcite plate in an aqueous solution with SDS and 5 mM NaCl, the equilibrium separation is found to be at about 46 nm.

A video microscopy setup as depicted in Fig. 6(b) is suggested to track the disk's motion. Placing the disk between crossed polarizers, allows one to determine the orientation of the optic axis by measuring the intensity of the transmitted light. The intensity in the setup can be shown to be given by

$$I \propto \frac{1}{2}[1 - 2\cos(2\theta)]\sin(\phi), \tag{16}$$

where $\phi = 2\pi h\Delta n/\lambda$ is the phase retardation due to the birefringent disk with thickness h and a birefringence of Δn for light of wavelength λ. For an initial trial of the experiment, the particle tracking has been explored using 10 μm diameter spheres in an aqueous solution. The Brownian motion of the spheres was recorded via a CCD camera attached to an upright microscope. The right part of Fig. 6(b) shows the tracking and the intensity fluctuations recorded for one particle. As the spheres are nonbirefringent, the recorded intensity fluctuations are solely due to scattering from imperfections in the spheres as they undergo Brownian motion.

4.3. *Three-threaded pendulum*

In Ref. 45, the Casimir torque between two nanostructured plates has been investigated. It was found that for lamellar gratings with a period of 400 nm, filling factor of 1/2 and corrugation height of 200 nm at a separation of 100 nm the Casimir torque per area is 3.5×10^{-8} N m^{-1} for a twist angle of about $\theta \approx 12.5°$. This value of the torque is orders of magnitude larger than what is typically observed for planar anisotropic plates (cf. Fig. 1(b)). Besides the theoretical results, an experimental setup capable of measuring torques of this order of magnitude was proposed.

The experimental setup depicted in Fig. 6(c) is composed of a marionette (thin cylindrical plate in plane A) suspended above a substrate (grounded plate). The relative positioning between the two plates can be controlled using a piezo-stage. At small enough separations, the two plates essentially interact through the Casimir energy. While the experiment is proposed for nanostructured plates, it can be used to measure the Casimir interaction for other systems with a similar magnitude of the torque. In contrast to the experiments proposed in Subsecs. 4.1 and 4.2, the interacting plates are in vacuum and not immersed in a liquid.

The marionette is suspended by a separation of $\ell = 20$ cm from a rigid frame (in plane B) by three threads with a threefold rotational symmetry. The tripod-like setup has the advantage that its torsional spring constant does not depend on the intrinsic torsional spring constants of the individual threads. Moreover, if the separation of the supporting points (symbolic triangles on the left of Fig. 6(c)) on the marionette and the rigid frame are chosen small enough compared to the marionette radius, rotational and translational motion of the pendulum can be decoupled which is necessary for an observation of the Casimir torque. The decoupling can be achieved when the characteristic frequencies of the rotational oscillation ω_r are much smaller than the one for the translational oscillation ω_t. It can be shown that for this pendulum geometry those characteristic frequencies are related by $\omega_r^2/\omega_t^2 = 2ab/\rho^2$, where a and b are the separations of the supporting points of the threat from the symmetry axis in planes A and B, respectively, (see schematic triangles on the left of Fig. 6(c)) and ρ is the radius of the marionette. The decoupling condition can then be met for the choice of dimensions $a = 1$ mm, $b = 60$ μm and $\rho = 5$ mm.

With the characteristic frequency of the translational oscillation given by $\omega_t = \sqrt{g/\ell}$, g being the gravitational acceleration, the rotational frequency is smaller by a factor of 10 with $\omega_r/2\pi \approx 0.08$ Hz. The choice of the length scale a gives further freedom to tune ω_r to a specific frequency range. To isolate the rotations from most of the seismic background, it is important to choose a value for ω_r below the microseismic fundamental mode at $\sim$0.1 Hz.

The sensitivity of the experimental setup can be estimated through the limitations set by thermal fluctuations. From the Brownian angular noise spectrum the minimal detectable torque can be estimated. Assuming critical damping and low frequencies, the minimal detectable torque is then estimated to be

$\delta\tau_{\min} \sim \sqrt{4k_{\mathrm{B}}TI\omega_r}$ N m/$\sqrt{\mathrm{Hz}}$ with I being the moment of inertia of the marionette. With the realistic values of the experimental setup given above and assuming a typical mass of 0.5 g for the marionette, this corresponds to a value of about 10^{-14} N m/$\sqrt{\mathrm{Hz}}$, which falls well within the theoretical prediction of the theoretical result obtained for the two nanostructured plates given above.

Having estimated that this experimental setup is capable of measuring the Casimir torque, the angular change of the suspended plate can be measured with a weak laser beam reflected on the center of the plate onto a low-noise position-sensitive detector with a typical sensitivity of a few nrad/$\sqrt{\mathrm{Hz}}$. Alternatively, optical interferometers can be used, which can be made sensitive to both rotational and lateral displacement of the suspended plate.

It is of particular interest for this experiment that it allows the measurement of the Casimir torque in vacuum. A major challenge, however, is to maintain parallelism of the two interacting plates. This may be largely overcome by working with larger plate separations with the trade-off being a reduced Casimir torque intensity.

4.4. *Optical tweezer*

Another setup allowing the measurement of the Casimir torque in air or vacuum was proposed in Ref. 66. The proposed experiment consists of a cylindrical nanorod of 200 nm length and 40 nm diameter that is levitated above a birefringent plate using an optical tweezer. The nanorod is assumed to be made of silica. For the birefringent plate, barium titanate and calcite are considered in the proposed experiment. The setup is schematically depicted in Fig. 6(d).

It is demonstrated that the nanorod can be trapped with a linearly polarized, tightly focused laser beam of wavelength 1064 nm and 100 mW power. The trapping potential is calculated to be about 2.2×10^4 K $\cdot k_{\mathrm{B}}$ at the center of the Gaussian beam, which is assumed to be 266 nm away from the plate. The trapping is thus stable against thermal fluctuations, and it is shown that the potential is a few orders of magnitude larger than the Casimir energy at that separation. At the trapping separation, the maximal Casimir torque is calculated to be around 3.2×10^{-25} N m for barium titanate and around 4.6×10^{-24} N m for calcite. The Casimir force for both plate materials is found to be at about 10^{-16} N.

The sensitivity of the setup can be estimated through two sources of noise. The first source is due to thermal fluctuations due to the gas surrounding the nanorod and the second is due to the recoil of scattered photons from the laser light. While the former is more relevant at higher pressures of the gas, the latter gives the main contribution of noise for a high vacuum. It is estimated that the turning point between these two regimes is at a pressure of about 10^{-7} Torr. At room temperature and a pressure of 10^{-7} Torr, the sensitivity for the Casimir torque is at about 10^{-28} N m/$\sqrt{\mathrm{Hz}}$ and while the sensitivity for the Casimir force is at about 10^{-21} N/$\sqrt{\mathrm{Hz}}$. For measuring times of 1 s, the Casimir torque and force are thus expected to be measurable within this optical tweezer setup.

As the nanorod changes polarization of the laser beam, its angular orientation can be detected with a polarizing beam splitter (PBS) and a balanced detector. The static change of polarization due to the birefringent plate can be cancelled by a tunable waveplate as shown on the right of Fig. 6(d).

The measurement of the Casimir force and torque can be affected by surface roughness of the probes and the existence of surface patch potentials. Because the roughness can be controlled to be less than 3 nm by polishing, the Casimir torque due to surface roughness can be neglected.

While levitated nanoparticles have typically no charge, patch potentials on the birefringent plate can cause a force or a torque on the nanoparticles due to the induced dipole. As patch potentials have a fixed position on the plate, it is demonstrated that the influence of such patch potentials on the measurement of the torque can be averaged out by sampling at different locations. With only 30 sampling points along a line, the average torque due to a typical patch potential is shown to be three orders of magnitude smaller than the value of the Casimir torque. The influence of roughness and patch potentials can be further minimized by characterization of the plate surface through Kelvin force microscopy because an area with small roughness and patch potential can be chosen for the measurement.

The proposed setup not only potentially allows a measurement of the Casimir torque in vacuum or across air, but due to its high sensitivity it is capable of measuring the torque at relatively large separations of more than 200 nm. Moreover, the system may be used for other high-precision measurements.

5. Experimental Verification

In Ref. 11, the Casimir torque was measured for the first time. The experimental setup is depicted in Fig. 7(a). The interacting surfaces are a liquid crystal (5CB) and a solid birefringent plate ($CaCO_3$, $LiNbO_3$, TiO_2 or YVO_4) separated by isotropic layers of Al_2O_3 and FC-4430. The design builds on a previously proposed geometry[39] and allows a precise optical detecting of the liquid crystal rotation due to the Casimir torque.[40]

On the opposite side of the interacting surfaces, the liquid crystal is anchored with an angle θ_{rub} (measured relative to the extraordinary axis of the birefringent substrate) onto a glass slide. This anchoring is induced by a rubbing a polyvinyl alcohol (PVA) coating on the glass slide. To eliminate liquid-crystal sticking at the top and bottom interfaces, FC-4430 is added to the 5CB.

The Casimir torque acts on the 5CB molecules near the solid crystal interface and induces a rotation through the bulk of the liquid crystal. Using the Oseen–Frank free energy, one can estimate the restoring torque per unit area of the elastic bulk to be[40]

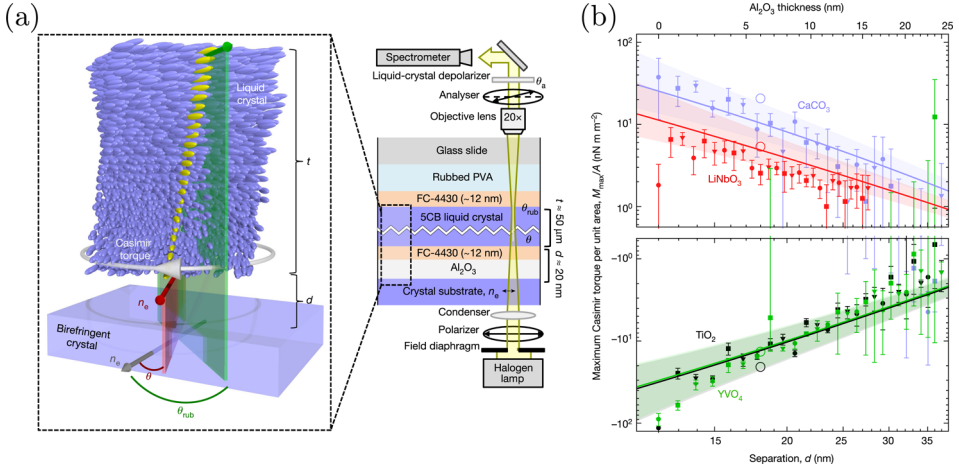$$M_{\mathrm{elastic}} = \frac{k_{22}\Delta\theta}{t} \tag{17}$$

Fig. 7. (Color online) Experimental measurement of the Casimir torque. (a) Schematic experimental setup to measure the Casimir torque. (b) Measured Casimir torque at a twist angle of $\theta = \pi/4$ between 5CB and four birefringent substrates — CaCO$_3$ (purple), LiNbO$_3$ (red), TiO$_2$ (black) and YVO$_4$ (green) — as a function of separation d. The separation includes the known Al$_2$O$_3$ thickness and a constant offset of 12 nm due to the surfactant and surface roughness. Solid lines represent the theoretical prediction of the torque with the shaded region corresponding to the range of values for the offset between 8 and 16 nm. The different symbols correspond to different samples of the same materials. (adapted from Ref. 11)

with the elastic constant of the twist $k_{22} \approx 3.6$ pN, the measured thickness of the liquid-crystal layer $t \approx 50$ μm, and the twist angle $\Delta\theta = \theta_{\text{rub}} - \theta$. As the Casimir torque and the elastic torque M_{elastic} are at balance, one can deduce the Casimir torque in the experimental setup by optically measuring the twist angle $\Delta\theta$ using polarized microscopy.

The resulting measured Casimir torque has a $\sin(2\theta)$ dependence. Figure 7(b) shows the measured maximum Casimir torque at $\theta = \pi/4$. The experimental values are given by the filled symbols with corresponding error bars. Different symbols of the same color correspond to different samples of the same configuration. The solid lines represent the theoretical prediction based on formula (11) where an additional offset on the Al$_2$O$_3$ layer of 12 nm is assumed due to the surfactant. The shaded area corresponds to values of this offset from 8 nm to 16 nm. As can be seen from the figure, the theoretical predictions and the experimental, measured magnitude of the Casimir torque and its sign match very well for all the plate materials considered.

6. Conclusions and Outlook

In this paper, we have reviewed the latest progress in the Casimir torque. For uniaxial birefringent plates, we have discussed the theoretical framework of calculating the Casimir torque and applied it the interaction between typical anisotropic materials. Moreover, we have reviewed theoretical predictions of the Casimir torque for various systems. Earlier proposed setups for measuring the Casimir torque were

discussed and finally we have reviewed the so far only experimental verification of the Casimir torque.

Overall the Casimir torque has been less explored than the Casimir force both on the theoretical and experimental fronts leaving many further opportunities for an exploration of these unique predictions of quantum electrodynamics.

Acknowledgment

References

1. M. Bordag, G. Klimchitskaya, U. Mohideen and V. Mostepanenko, *Advances in the Casimir Effect* (Oxford University Press, 2009).
2. R. Decca, V. Aksyuk and D. López, Casimir force in micro and nano electro mechanical systems, in *Casimir Physics*, eds. D. Dalvit, P. Milonni, D. Roberts and F. da Rosa, Lecture Notes in Physics, Vol. 834, Chap. 9 (Springer, 2011), p. 287.
3. T. Gong, M. R. Corrado, A. R. Mahbub, C. Shelden and J. N. Munday, *Nanophotonics* **10**, 523 (2021), doi:10.1515/nanoph-2020-0425.
4. H. B. G. Casimir, *Proc. Kon. Ned. Akad. Wetenschappen* **51**, 79 (1948).
5. E. M. Lifshitz, *Sov. Phys. JETP* **2**, 73 (1956).
6. I. Dzyaloshinskii, E. Lifshitz and L. Pitaevskii, *Adv. Phys.* **10**, 165 (1961), doi:10.1080/00018736100101281.
7. S. J. van Enk, *Phys. Rev. A* **52**, 2569 (1995), doi:10.1103/PhysRevA.52.2569.
8. E. I. Kats, *Sov. Phys. JETP* **33**, 634 (1971).
9. V. A. Parsegian and G. H. Weiss, *J. Adhesion* **3**, 259 (1972), doi:10.1080/00218467208072197.
10. Y. S. Barash, *Radiophys. Quantum Electron.* **21**, 1138 (1978), doi:10.1007/BF02121382.
11. D. A. T. Somers, J. L. Garrett, K. J. Palm and J. N. Munday, *Nature* **564**, 386 (2018), doi:10.1038/s41586-018-0777-8.
12. F. Capasso, J. N. Munday, D. Iannuzzi and H. B. Chan, *IEEE J. Select. Top. Quantum Electron.* **13**, 400 (2007), doi:10.1109/JSTQE.2007.893082.
13. F. Capasso and J. N. Munday, Attractive and repulsive Casimir–Lifshitz forces, QED torques, and applications to nanomachines, in *Casimir Physics*, eds. D. Dalvit, P. Milonni, D. Roberts and F. da Rosa, Lecture Notes in Physics (Springer, Berlin, Heidelberg, 2011), pp. 249–286.
14. B.-S. Lu and R. Podgornik, *J. Chem. Phys.* **145**, 044707 (2016), doi:10.1063/1.4959282.
15. R. Zeng, C. Wang, X. Zeng, H. Li, S. Yang, Q. Li and Y. Yang, *Opt. Exp.* **28**, 7425 (2020), doi:10.1364/OE.386083.
16. W. Broer, B.-S. Lu and R. Podgornik, *Phys. Rev. Res.* **3**, 033238 (2021), doi:10.1103/PhysRevResearch.3.033238.
17. D. M. Dryden, J. C. Hopkins, L. K. Denoyer, L. Poudel, N. F. Steinmetz, W.-Y. Ching, R. Podgornik, A. Parsegian and R. H. French, *Langmuir* **31**, 10145 (2015), doi:10.1021/acs.langmuir.5b00106.
18. A. Lambrecht, P. A. Maia Neto and S. Reynaud, *New J. Phys.* **8**, 243 (2006), doi:10.1088/1367-2630/8/10/243.

19. S. J. Rahi, T. Emig, N. Graham, R. L. Jaffe and M. Kardar, *Phys. Rev. D* **80**, 085021 (2009), doi:10.1103/PhysRevD.80.085021.

20. D. A. T. Somers and J. N. Munday, *Phys. Rev. A* **95**, 022509 (2017), doi:10.1103/PhysRevA.95.022509.

21. W. Broer, J. Y. H. Liow and B.-S. Lu, *Phys. Rev. A* **100**, 012514 (2019), doi:10.1103/PhysRevA.100.012514.

22. J. Lekner, *J. Phys.: Condens. Matter* **3**, 6121 (1991), doi:10.1088/0953-8984/3/32/017.

23. J. Lekner, *J. Opt. Soc. Am. A* **10**, 2059 (1993), doi:10.1364/JOSAA.10.002059.

24. J. N. Munday, D. Iannuzzi, Y. Barash and F. Capasso, *Phys. Rev. A* **71**, 042102 (2005), doi:10.1103/PhysRevA.71.042102.

25. J. N. Munday, D. Iannuzzi, Y. Barash and F. Capasso, *Phys. Rev. A* **78**, 029906 (2008), doi:10.1103/PhysRevA.78.029906.

26. T. G. Philbin and U. Leonhardt, *Phys. Rev. A* **78**, 042107 (2008), doi:10.1103/PhysRevA.78.042107.

27. J. C. Hopkins, R. Podgornik, W.-Y. Ching, R. H. French and V. A. Parsegian, *J. Phys. Chem. C* **119**, 19083 (2015), doi:10.1021/acs.jpcc.5b01870.

28. D. A. Somers and J. N. Munday, *Phys. Rev. Lett.* **119**, 183001 (2017), doi:10.1103/PhysRevLett.119.183001.

29. P. Thiyam, P. Parashar, K. Shajesh, O. I. Malyi, M. Boström, K. A. Milton, I. Brevik and C. Persson, *Phys. Rev. Lett.* **120**, 131601 (2018), doi:10.1103/PhysRevLett.120.131601.

30. L. Chen and K. Chang, *Phys. Rev. Lett.* **125**, 047402 (2020), doi:10.1103/PhysRevLett.125.047402.

31. J. C. Martinez, X. Chen and M. B. A. Jalil, *AIP Adv.* **8**, 015330 (2018), doi:10.1063/1.5007787.

32. P. Thiyam, P. Parashar, K. V. Shajesh, O. I. Malyi, M. Boström, K. A. Milton, I. Brevik, J. Forsman and C. Persson, *Phys. Rev. B* **100**, 205403 (2019), doi:10.1103/PhysRevB.100.205403.

33. B.-S. Lu, *Phys. Rev. B* **97**, 045427 (2018), doi:10.1103/PhysRevB.97.045427.

34. F. Lindel, G. W. Hanson, M. Antezza and S. Y. Buhmann, *Phys. Rev. B* **98**, 144101 (2018), doi:10.1103/PhysRevB.98.144101.

35. R. Esquivel-Sirvent, G. H. Cocoletzi and M. Palomino-Ovando, *J. Appl. Phys.* **108**, 114101 (2010), doi:10.1063/1.3514152.

36. G. Deng, Z.-Z. Liu and J. Luo, *Phys. Rev. A* **80**, 062104 (2009), doi:10.1103/PhysRevA.80.062104.

37. C.-G. Shao, D.-L. Zheng and J. Luo, *Phys. Rev. A* **74**, 012103 (2006), doi:10.1103/PhysRevA.74.012103.

38. K. Yasui and K. Kato, *J. Phys. Chem. C* **119**, 24597 (2015), doi:10.1021/acs.jpcc.5b06798.

39. E. Smith and B. Ninham, *Physica* **66**, 111 (1973), doi:10.1016/0031-8914(73)90267-X.

40. D. A. T. Somers and J. N. Munday, *Phys. Rev. A* **91**, 032520 (2015), doi:10.1103/PhysRevA.91.032520.

41. M. Antezza, H. Chan, B. Guizal, V. N. Marachevsky, R. Messina and M. Wang, *Phys. Rev. Lett.* **124**, 013903 (2020), doi:10.1103/PhysRevLett.124.013903.

42. R. Esquivel-Sirvent and G. C. Schatz, *J. Phys. Chem. C* **117**, 5492 (2013), doi:10.1021/jp400581j.

43. R. B. Rodrigues, P. A. M. Neto, A. Lambrecht and S. Reynaud, *Europhys. Lett.* **76**, 822 (2006), doi:10.1209/epl/i2006-10340-1.

44. R. B. Rodrigues, P. A. M. Neto, A. Lambrecht and S. Reynaud, *J. Phys. A: Math. Theor.* **41**, 164019 (2008), doi:10.1088/1751-8113/41/16/164019.

45. R. Guérout, C. Genet, A. Lambrecht and S. Reynaud, *Europhys. Lett.* **111**, 44001 (2015), doi:10.1209/0295-5075/111/44001.

46. V. A. Parsegian, *J. Chem. Phys.* **56**, 4393 (1972), doi:10.1063/1.1677878.

47. R. F. Rajter, R. Podgornik, V. A. Parsegian, R. H. French and W. Y. Ching, *Phys. Rev. B* **76**, 045417 (2007), doi:10.1103/PhysRevB.76.045417.

48. A. Šiber, R. F. Rajter, R. H. French, W. Y. Ching, V. A. Parsegian and R. Podgornik, *Phys. Rev. B* **80**, 165414 (2009), doi:10.1103/PhysRevB.80.165414.

49. P. Rodriguez-Lopez and T. Emig, *Phys. Rev. A* **85**, 032510 (2012), doi:10.1103/PhysRevA.85.032510.

50. J. F. Dobson, T. Gould and I. Klich, *Phys. Rev. A* **80**, 012506 (2009), doi:10.1103/PhysRevA.80.012506.

51. T. A. Morgado, S. I. Maslovski and M. G. Silveirinha, *Opt. Exp.* **21**, 14943 (2013), doi:10.1364/OE.21.014943.

52. A. Ashourvan, M. Miri and R. Golestanian, *Phys. Rev. Lett.* **98**, 140801 (2007), doi:10.1103/PhysRevLett.98.140801.

53. S. Sanders, W. J. M. Kort-Kamp, D. A. R. Dalvit and A. Manjavacas, *Commun. Phys.* **2**, 71 (2019), doi:10.1038/s42005-019-0163-3.

54. A. Weber and H. Gies, *Phys. Rev. D* **80**, 065033 (2009), doi:10.1103/PhysRevD.80.065033.

55. J.-G. Guo and Y.-P. Zhao, *J. Microelectromech. Syst.* **13**, 1027 (2004), doi:10.1109/JMEMS.2004.838390.

56. F. Tajik, M. Sedighi and G. Palasantzas, *J. Appl. Phys.* **121**, 174302 (2017), doi:10.1063/1.4982762.

57. F. Tajik, M. Sedighi, M. Khorrami, A. A. Masoudi and G. Palasantzas, *Phys. Rev. E* **96**, 042215 (2017), doi:10.1103/PhysRevE.96.042215.

58. F. Tajik, M. Sedighi, A. A. Masoudi, H. Waalkens and G. Palasantzas, *Phys. Rev. E* **98**, 022210 (2018), doi:10.1103/PhysRevE.98.022210.

59. F. C. Lombardo, F. D. Mazzitelli and P. I. Villar, *J. Phys. A: Math. Theor.* **41**, 164009 (2008), doi:10.1088/1751-8113/41/16/164009.

60. I. Cavero-Peláez, K. A. Milton, P. Parashar and K. V. Shajesh, *Phys. Rev. D* **78**, 065019 (2008), doi:10.1103/PhysRevD.78.065019.

61. M. Shahzamani, M. Amini and M. Soltani, *Eur. Phys. J. D* **71**, 13 (2017), doi:10.1140/epjd/e2016-70042-8.

62. V. Vaidya, *Phys. Rev. A* **90**, 022105 (2014), doi:10.1103/PhysRevA.90.022105.

63. S. J. Rahi and S. Zaheer, *Phys. Rev. Lett.* **104**, 070405 (2010), doi:10.1103/PhysRevLett.104.070405.

64. M. Antezza, I. Fialkovsky and N. Khusnutdinov, *Phys. Rev. B* **102**, 195422 (2020), doi:10.1103/PhysRevB.102.195422.

65. J. N. Munday, D. Iannuzzi and F. Capasso, *New J. Phys.* **8**, 244 (2006), doi:10.1088/1367-2630/8/10/244.

66. Z. Xu and T. Li, *Phys. Rev. A* **96**, 033843 (2017), doi:10.1103/PhysRevA.96.033843.

67. J. N. Munday, F. Capasso and V. A. Parsegian, *Nature* **457**, 170 (2009), doi:10.1038/nature07610.